Pressure Drop Decrease and Heat Transfer Increase in the Internal Flow Using a New Geometry

Ahmad Bedram

Assistant Professor, Department of Mechanical Engineering, Technical and Vocational University (TVU), Tehran, Iran
Email: abedram@tvu.ac.ir
Postal code: 1435763811
Tel: +985632828274
Mobile:

Abstract

This paper presented investigates nanofluid heat transfer inside the channel. The considered fluid was a nanofluid consisting of water and aluminum oxide nanoparticles. Nanofluid volume fraction from 0 to 4% and Reynolds numbers from 5 to 700 have been investigated. Numerous numerical results have been obtained, including: velocity profile, temperature, pressure and Nusselt number. Pressure, velocity and temperature contours were also presented and streamlines were drawn at different Reynolds numbers. The geometry of this research, decreases the pressure drop. For example, at a Reynolds number of 200, the fluid temperature increase in the geometry of this paper was %181 higher than that of a simple tube (with similar conditions), and the pressure drop was 19% lower than the pressure drop of a simple tube. Also a stagnation point was formed in the flow, where the highest pressure in the problem occurred at that point.

Keywords: Internal flow, Numerical simulation, Nanofluid, Heat transfer enhancement, Pressure drop decrease,

1. Introduction

Heat transfer is a phenomenon that occurs in many industrial processes. Heat transfer control in such processes can increase process efficiency and bring good economic savings. Heat transfer in closed chambers [1], heat transfer in solar water heaters [2], increasing heat transfer using surface roughness adjustment [3], increasing heat transfer in evaporators [4], increasing heat transfer in heat exchangers [5, 6] are examples of the application of heat transfer in industries.

Various methods have been proposed to improve heat transfer in the internal flow. In one of these methods, obstacles of different shapes are placed in the flow field and heat transfer increases by generating turbulence in the flow [7, 8]. In another method, the tube is made in a wavy or sinusoidal shape and heat transfer increases by vorticity generation in the flow field [9-11]. In another method, adding twisted tape inside the channel increases the heat transfer [12, 13]. In some methods, heat transfer increases by adding nanoparticles of a metal to the water flow inside the channel [14-16] or adding a magnetic field [17] or using the channel with various cross sections [18] or adding circular cylinders inside a channel [19] or investigating porous channels with various cross sections [20] or using wavy channel [21].

Mousa et al. [22] in a review study discussed the heat transfer increasing methods in single-phase flow. They used various obstacles inside the channel.

Mashoofi and pourahmad [23] investigated the effect of a wire turbulator vibration on the nanofluid heat transfer in a channel. They considered a specific frequency for the wire vibration. Also, they investigated the

effect of mass flow rate. Their results showed that the nanofluid with vibrating wire turbulator increased the heat transfer coefficient up to %150.

Ma et al. [24] investigated the condensation heat transfer in pipe flow with fins. They fined the heat transfer coefficient of finned pipe was 1.5 to 2.2 times higher than the simple tube. Also, they stated that the pressure drop increased monotonically with mass flow rate.

yuan et al. [25] investigated the heat transfer in a channel with twisted fins. Their research method was experimental and numerical simulation. They stated by increase the umber of winglets from 2 to 14, the heat transfer coefficient and friction factor increase %7.9 and %24.5 respectively. Also, they developed a correlation between Nusselt number and friction factor.

Naga Ramesh et al. [26] investigated methods of increasing heat transfer in microscale channels. They used an obstacle in the flow field and used a magnetic field.

Akbarzadeh and Valipour [27] investigated the heat transfer improvement using helically corrugated tubes. They stated that the use of corrugated tube increased the heat transfer between 85 and 107% and the friction coefficient between 25 and 85%.

Nguyen et al. [28] investigated the effect of adding a triangular obstacle on heat transfer from the tube as well as the effect of the magnetic field on the flow. Their results showed that the addition of the triangular obstacle increased the heat transfer rate. But at high Re, the triangular obstacles created vortexes in the flow.

Wang et al. [29] studied the heat transfer in a channel with a stair. They considered several different geometries for their stairs. They used numerical simulation and showed that the "NR" geometry mode had no effect on the heat transfer increase and pressure drop. The geometry with ribs had a significant effect on heat transfer increase.

Zhang K. et al. [30] investigated the heat transfer in the tube by adding a ring with rectangular ribs. Their geometry was investigated in two “parallel” and “V-shaped” modes. Their results showed that the parallel mode created a longitudinal vortex and the V-shaped mode created several longitudinal vortexes, and both modes increased flow turbulence.

This paper presents a new geometry to increase the heat transfer of internal nanofluid flow. we name this geometry: “long obstacle geometry”. In the geometry of this research, in addition to increasing the heat transfer, the pressure drop of the system also decreased (except at high Re). Water-aluminum oxide nanofluid is considered in this geometry. The heat transfer of the geometry of this research is more than the heat transfer of a simple tube with similar conditions. Also, the pressure drop of the geometry of this paper, in a significant range of the Re, is lower than the pressure drop of a simple tube. But in many methods presented in previous researches, heat transfer increase has also led to an increase in pressure drop. Grid independency has been done and the numerical results have been compared with the results of an experimental study. Reynolds numbers from 5 to 700 and volume fraction of nanoparticles between 0 and 4% are investigated. The temperature profile, velocity and pressure in different Re, different volume fractions of nanofluid and in different locations of the geometry are presented. The changes of Nusselt number in different Re and different volume fractions are also presented. In different Re, the heat transfer increase of the proposed geometry compared to the simple tube and the pressure drop of the proposed geometry compared to the simple tube.

2. Specifications

In the problem of this research, the flow is steady and incompressible. Also the continuity, momentum and energy equations are established as follows [31, 32]:

$$\frac{\partial u_i}{\partial x_i} = 0 \tag{1}$$

$$\rho\left(\frac{\partial u_i}{\partial t} + u_j \frac{\partial u_i}{\partial x_j}\right) = \rho g_i - \frac{\partial p}{\partial x_i} + \mu \frac{\partial^2 u_i}{\partial x_j^2} \tag{2}$$

$$\frac{\partial (u_i T)}{\partial x_i} = \frac{k}{\rho c_p} \frac{\partial^2 T}{\partial x_i^2} \tag{3}$$

where k, ρ and c_p are defined in the nomenclature. Numerical simulation was done using the Ansys Fluent v.15. The condition for completing the numerical solution is that the residuals become smaller than 0.0007. The geometry is created and meshed in Gambit. The grid size near the walls is reinforced.

Discretization of momentum and energy equations is performed by the second order upwind method, and pressure-velocity coupling is performed by the SIMPLEC algorithm. The flow is laminar and the inlet boundary condition is constant velocity and outlet boundary condition is constant pressure and wall boundary condition is no-slip. The thermal boundary condition in the walls is a constant heat flux equal to 10,000W/m^2.

Figure 1 shows the proposed geometry. The geometry is axisymmetric. The diameter of the inlet and outlet channels is 90 μm. In the middle of the geometry, there is an obstacle of 130 μm height.

The following equations can be used to calculate the specifications of nanofluid [33]:

$$\begin{aligned}
&\rho_{nf} = \varphi\rho_p + (1-\varphi)\rho_{bf} \\
&\frac{k_{nf}}{k_{bf}} = 4.97\varphi^2 + 2.72\varphi + 1 \\
&\frac{\mu_{nf}}{\mu_{bf}} = 123\varphi^2 + 7.3\varphi + 1 \\
&c_{nf} = \frac{\varphi\rho_p c_p + (1-\varphi)\rho_{bf} c_{bf}}{\rho_{nf}}
\end{aligned} \tag{4}$$

where φ, k, ρ, μ, c and subscripts are defined in the nomenclature.

The fluid considered for this problem is a nanofluid of water and Al_2O_3. The specifications of water and Al_2O_3 are as follows [33, 34]:

$$\begin{aligned}
&\rho_{water} = 997.13\frac{kg}{m^3} \qquad k_{water} = 0.606\frac{W}{m^\circ K} \\
&c_{water} = 4179\frac{J}{kg^\circ K} \qquad \mu_{water} = 0.00089\frac{kg}{ms} \\
&\rho_{Al_2O_3} = 3970\frac{kg}{m^3} \qquad k_{Al_2O_3} = 40\frac{W}{m^\circ K} \\
&c_{Al_2O_3} = 765\frac{J}{kg^\circ K}
\end{aligned} \tag{5}$$

Using equations 4 and 5, the specifications of the nanofluid of water and 2% Al_2O_3 nanoparticles will be as follows:

$$\begin{aligned}
&\rho_{water-Al_2O_3(2\%)} = 1056.59\frac{kg}{m^3} \\
&k_{water-Al_2O_3(2\%)} = 0.6401711\frac{W}{m^\circ K} \\
&\mu_{water-Al_2O_3(2\%)} = 0.0010637\frac{kg}{ms} \\
&c_{water-Al_2O_3(2\%)} = 3922.45\frac{J}{kg^\circ K}
\end{aligned} \tag{6}$$

Reynolds number of nanofluid is defined as follows [16]:

$$\mathrm{Re}_{nf} = \frac{\rho_{nf}\bar{U}D}{\mu_{nf}} \tag{7}$$

Where ρ, μ, D, $\bar{U}$ and nf are defined in the nomenclature.

3. Validation

The nanofluid of water and 3.5% Al_2O_3 is considered in the geometry of the problem at a Re=100 to examine the grid independency. The results have been compared in four grids of different sizes. Figure 2 compares the temperature profile in the section x=1000 μm in four different grids. Nusselt number is defined as $Nu=h_{nf}d_{nf}/k_{nf}$ where h, d and k are defined in the nomenclature. As can be seen, for grids more than 7403nodes, the results are grid independent.

The numerical results of this paper have been compared with the experimental results of Kim et al. [35] to validate the numerical simulation. In the paper of Kim et al. [35], the flow of nanofluid of water and 3% Al_2O_3 in a tube with a diameter of 4.57 mm and a length of 2 m and a Re=1460, which has a wall with a constant heat flux, was investigated; and the heat transfer coefficient along the length of the tube was reported. In Figure 3, the numerical (this paper) and experimental [35] results of the heat transfer coefficient along the tube are compared. According to the figure, there is a good agreement between the results of the two papers.

4. Results and discussion

The 3D image of the geometry is shown in Figure 4. In the geometry, there is an obstacle marked in black. we name this geometry: "long obstacle geometry". The height of this obstacle is 130 μm and it is well shown in Figure 1.

4-1 Investigation of the effect of nanofluid volume fraction

Figure 5 shows the velocity magnitude profile in different nanofluid volume fractions at Re=100 and cross section x=450 μm. According to the figure, as the volume fraction of nanofluid increases, the maximum velocity also increases. So that for nanofluid with zero volume fraction, the maximum velocity is 0.0928m/s and for nanofluid with 4% volume fraction, the maximum velocity is 0.126m/s (the difference is about 36%). In Figure 5, the streamlines are shown for the volume fraction of 4%. As can be seen, two large vortexes are formed before the obstacle. The fluid flow also passes through the middle of these two vortexes and the highest velocity occurs in the place between the two vortexes (which is also marked with a red oval in the figure). Naturally, due to the no-slip boundary condition in walls, the velocity at the location of the walls is zero.

Figure 6 shows the temperature profile in different nanofluid volume fractions at Reynolds 100 and cross-section x=450 μm. According to the figure, the nanofluid volume fraction has a negligible effect on the temperature profile. In the small diagram drawn in Figure 6, the mean temperature is presented as a function of nanofluid volume fraction. According to this diagram, the mean temperature for nanofluid with 0% volume fraction (i.e. pure water) is 300.366^{o}K and for 4% volume fraction is 300.301^{o}K. In other words, the difference between the mean fluid temperature for a volume fraction of 0% and 4% is about 0.02%. Also, according to Figure 6, the maximum temperature is related to the points $y/D_{in}=\pm 2.7$. Because these points are located on the wall of the geometry and the wall has a constant heat flux.

Figure 7 shows the diagram of pressure profile in different nanofluid volume fractions at Reynolds number 100 and cross section x=450 μm. According to the figure, with the increase of volume fraction of nanofluid, fluid pressure increases. The reason for this is that as the volume fraction of nanofluid increases, the system pressure drop increases. On the other hand, the boundary condition of outlet is constant pressure and is equal to the ambient pressure. Therefore, as the pressure drop of the system increases, the inlet pressure increases. As a result, by increasing the inlet pressure, the pressure in other sections will also increase. The small diagram in Figure 7 shows the mean pressure as a function of nanofluid volume fraction. Also, according to the figure, the pressure across the channel width is almost constant and has little change.

Figure 8 shows "Nusselt number along the channel" in different nanofluid volume fractions. The origin of the coordinates and the geometric dimensions of the problem are shown in Figure 1. According to the figure, changing the nanofluid volume fraction has a negligible effect on the Nusselt number profile along the channel. However, with the increase of volume fraction of nanofluid, the Nusselt number increases slightly. For example, in the dimensionless location x/D=2, the Nusselt number for the volume fraction of 1% and 4% is 8.067 and 8.567, respectively (about 6% increase). The inlet tube (i.e. $0<x/D<2$) and the outlet tube ($10<x/D<12$) have the highest

Nusselt number along the channel, because in these two parts, the fluid velocity and as a result the Reynolds number will have the highest value.

4-2. Investigation of the effect of Reynolds number

Figure 9 shows the velocity magnitude profile in different Re for nanofluid with a volume fraction of 3% at x=450 µm. As shown in the figure, at low Re, the velocity magnitude changes are small. Reynolds number 700 has the most velocity fluctuations. For Re=700, the streamlines are also drawn on the top of the figure. According to the figure, there are two large vortexes before the obstacle through which the fluid flows. The region between these two vortexes is called region 2. The highest velocity at Reynolds number 700 corresponds to this region, and it is marked with a blue oval in the figure. Also, the regions near the center of the vortexes have low velocity, and one of these regions is named region1 marked with a green oval in the figure.

Figure 10 shows the temperature profile in different Re for nanofluid with a volume fraction of 3% in cross section x=450 µm. The velocity contour is also shown inside the figure. According to the figure, as the Re increases, the temperature of the fluid decreases, because as Re increases, the opportunity for heat exchange between the fluid and the wall will decrease, therefore the temperature of the fluid will decrease. According to the figure, the maximum temperature in the problem is 305.74^{o}K, which occurs at Reynolds number 5 and at the wall location. At Re=5 and Re=10, the location of the lowest temperature is shown with black and red ovals. The fluid velocity in this region and its distance from the walls are high. Therefore, the lowest temperature occurs in this region (the contour inside Figure 10 shows that the fluid velocity is high in this region).

Figure 11 shows the fluid pressure profile in different Re for nanofluid with a volume fraction of 3% in cross-section x=450 µm. According to the figure, at Re<400, the fluid pressure along the channel width is almost constant, because the flow along the channel width is very low. Therefore, according to the momentum equation, pressure changes will be insignificant. But at Re=700, large vortexes are created in the flow, so a significant flow is created along the channel width. Therefore, the pressure will also change along the channel width. As the Re increases, the fluid pressure also increases. Because when the Re increases, the system pressure drop increases due to the inertial effect. On the other hand, since the outlet pressure is constant, the inlet pressure will increase. Finally, as the inlet pressure increases, the pressure increases in all sections. In the small diagram shown in Figure 11, the mean fluid pressure is presented as a function of Re. The mean fluid pressure in Reynolds number 5 and 700 are 64Pa and 72091Pa, respectively. Fluid pressure changes increase with increasing Re. In other words, as the Re increases from 5 to 10, the fluid pressure also increases by about 2.1 times. But by increasing the Re from 200 to 400, the fluid pressure increases by 3.3 times.

Figure 12 shows the “Nusselt number along the channel” in different Re. The origin of the coordinates and the geometric dimensions of the problem are shown in Figure 1. According to the figure, at Re>200, near the obstacle ($4<x/D<6$), the Nusselt number has increased, and this region is marked with number 2 on the figure. It is because, the velocity of the fluid near the wall increases in this region due to the formation of large vortexes. Also, in the range of $2<x/D<2.5$, the Nusselt number has suddenly decreased significantly, and this region is also marked with No. 1 in the figure. The reason for this is that at $x/D=2$, the flow is separated from the inlet channel. Therefore, the fluid velocity will be negligible near the wall. For this reason, the Nusselt number is greatly reduced. Also, according to the figure, in the location of x/D≈10, the Nusselt number slightly increases (this region is marked with No. 3 in the figure), which is due to the flow entering the outlet channel and increasing the fluid velocity.

4-3 Investigation of flow in different sections

In this section, we will examine the flow and heat transfer at different sections of the geometry of the problem.

Figure 13 shows the velocity magnitude contour at Reynolds number 300 and nanofluid with 3% volume fraction. The maximum velocity is approximately 5.53 m/s, which occurs at the center of the outlet tube.

Figure 14 shows the velocity magnitude profile in different sections for nanofluid with volume fraction 3% and Reynolds number 300. The selected sections and velocity magnitude contour are shown in the figure. Among the selected sections, the highest velocity corresponds to section x/D=4, which is equal to 2.79 m/s, and its location is shown with No. 3 and a red dashed line inside the figure. In section x/D=7, the maximum velocity is 1.1m/s, and its location is indicated by No. 2 and the black dashed line. The reason for the occurrence of the maximum velocity in region 2 is the narrowing of the channel at the location of the obstacle and the increase of the fluid

velocity due to passing through the obstacle. In the section x/D=5, the maximum velocity is 0.91m/s, and its location is indicated by No. 1 and the pink dashed line.

Figure 15 shows the temperature contour at Reynolds number 300 and nanofluid with a volume fraction of 3%. The maximum temperature is 301K and its location is on the wall (after the obstacle).

Figure 16 shows the temperature profile in different sections for nanofluid with a volume fraction 3% and a Reynolds number 300. Selected sections and temperature contour are shown inside the figure. According to the figure, the highest temperature is approximately 300.95^{o}K and corresponds to the section x/D=7 and occurs on the wall. Its exact location is marked on the figure with No. 3 and a red dashed line. The reason for the maximum temperature in this region is that in this region the fluid velocity is very low due to the presence of the obstacle (see Figure 13). On the other hand, this region is near the wall, and the wall also has a constant flux thermal boundary condition. Therefore, the temperature of this region increases more than other regions. Also, at the cross-section x/D=3, the highest temperature is approximately 300.52^{o}K and occurs at the wall, the exact location of which is shown on the figure with No. 2 and the blue dashed line. In the curve x/D=3, a fracture has occurred at the dimensionless location y/D_{in}=-0.6, and the location of this fracture is shown in the figure with No. 1 and a black dashed line. The reason for this is that this location is the boundary between the inlet flow and a vortex. On the side where the inlet flow is located, the temperature is low and on the side where the vortex is located, the temperature is high due to the low velocity of the fluid.

Figure 17 shows the pressure contour at Reynolds number 300 and nanofluid with a volume fraction of 3%. The maximum pressure occurs at the inlet as well as at point 1 (marked on the figure). At point 1, due to the direct impact of the flow on the wall, a stagnation point is created and the pressure rises.

Figure 18 shows the pressure profile in different sections for nanofluid with a volume fraction 3% and Reynolds number 300. Selected sections and pressure contours are shown in the diagram. In almost all sections (except for a small part of section x/D=3), the pressure changes along the channel width are negligible. In the curve x/D=5, in the region close to the wall, the pressure is slightly increased (this region is marked on the figure with No. 2 and the red dashed line). The reason for this increase in pressure is that in region 2, due to the presence of an obstacle, the fluid velocity is low, therefore the pressure slightly increases. According to the figure, the highest pressure occurs in the cross-section x/D=3 and in the center of the tube (i.e. y/D_{in}=0), which is marked with No. 1 and the blue dashed line on the figure. As mentioned before, the reason for the high pressure in region 1 is the formation of a stagnation point in this region.

4-4 Comparison of the performance of the geometry of this paper with a simple tube

In this section, the performance of the proposed geometry of this research is compared with a simple tube. For this purpose, a simple tube of a diameter of 90 μm is considered (the inlet diameter of the proposed geometry of this paper is also 90 μm). The length of the simple tube is also chosen to be 1080 μm (that is, the length of the geometry proposed in this paper). Nanofluid of water and 3% Al_2O_3 is considered. The results of the simple tube are extracted and compared with the results of the proposed geometry of this research. To compare the results of the simple tube and the proposed geometry, we define the quantity of dimensionless temperature as follows:

$$T^* = \frac{\Delta T_G - \Delta T_C}{\Delta T_C} \times 100 \tag{8}$$

Where ΔT_C is the increase in the mean temperature of the fluid passing through the simple tube and ΔT_G is the increase in the mean temperature of the fluid passing through the proposed geometry. The higher T^*, shows better thermal performance of this paper geometry than the simple tube. Also the higher T^* shows the greater ability to increase the fluid temperature.

We also define the quantity of dimensionless pressure as follows:

$$P^* = \frac{\Delta P_G - \Delta P_C}{\Delta P_C} \times 100 \tag{9}$$

Where ΔP_C is the pressure drop of the simple tube and ΔP_G is the pressure drop of the proposed geometry.

Figure 19 compares the pressure drop and thermal performance in the proposed geometry with the simple tube at different Re. According to the figure, in all the Re, "the fluid temperature increase" in the proposed geometry is

more than "the fluid temperature increase" in the simple tube. For example, at *Re*=200, "the fluid temperature increase" in the geometry of this paper is 181% more than "the fluid temperature increase" in a simple tube. Also, at *Re*=200, the pressure drop of the geometry of this paper is 19% lower than the pressure drop of the simple tube. Moreover, by reducing the Re, the performance of the geometry will also improve. For example, at Re=10, "the fluid temperature increase" in the geometry is 295% higher than "the fluid temperature increase" in a simple tube. Also, at a Re=10, the pressure drop of the geometry is 57% less than the pressure drop of a simple tube. Therefore, one of the important advantages of the proposed geometry of this research is that in addition to increasing the heat transfer, the pressure drop of the system is also reduced. But in a large number of methods proposed in previous researches, the increase in heat transfer has been accompanied by an increase in system pressure drop.

Figure 20 shows the streamlines for nanofluid with a volume fraction 3% at Reynolds numbers 50 to 700. According to the figure, as the Re increases, larger vortexes are formed in the flow. For example, at a Re=50, the width of the formed vortexes is about 100 μm, but at a Re=700, a vortex with a width of about 350 μm is formed before the obstacle. Also, with the increase of Re, the number of vortexes formed in the flow also increases. For example, 2 and 6 vortexes are formed at Reynolds numbers 50 and 700, respectively. The figure also shows that the presence of an obstacle has a great effect on the formation of vortexes, so that in all Re, large vortexes are formed after the obstacle, and even at higher Re (such as 700), two vortexes are formed after the obstacle.

Despite the advantages of the geometry of this paper, it has some disadvantages. For example, the manufacturing of the present geometry has higher cost than simple tube. We know that the existence of vortex in flow field, increases the pressure drop of the system. As seen in Fig. 20, with increase Reynolds number from 50 to 700 the vortex number in the flow field increases from 4 to 12. But there are no vortexes in a simple straight tube flow field. Therefore, the performance of the present geometry reduces with Reynolds number.

Fig. 21 shows the pressure drop and maximum temperature of the system as a function of Reynolds number. The pressure drop of the system increases with the Reynolds number. As stated in the previous paragraph the performance of the present geometry reduces with Reynolds number. But we should notice that in low Re, the maximum temperature of the system increases (Fig. 21). Increase of the maximum temperature can change the composition of the nanofluid, especially in the biofluid applications.

5. Conclusion

Heat transfer of a nanofluid of water and Al_2O_3 nanoparticles in a channel was examined in this paper. Nanofluid volume fraction from zero to 4% and Reynolds numbers from 5 to 700 were investigated. Grid independency was done and validation was also done and a good agreement was observed. Several numerical results were obtained, including: velocity profile, temperature, pressure and Nusselt number. Pressure, velocity and temperature contours were also presented and streamlines were drawn at different Re. In a large number of heat transfer increasing methods presented in previous researches, the pressure drop of the system also increased simultaneously with the increase of heat transfer. But the results of this research showed that in the proposed geometry, the pressure drop decreases. This was an important advantage of the proposed geometry. For example, at a Re=200, "the fluid temperature increase" in the geometry of this paper was 181% higher and the pressure drop was %19 lower than that of a simple tube with similar conditions. ***It was also found that by reducing the Reynolds number, the performance of the geometry also improved. For example, at Re=10, "the fluid temperature increase" in the geometry of this paper was 295% higher than "the fluid temperature increase" in a simple tube. Also, at a Re=10, the pressure drop of the geometry was 57% less than the pressure drop of a simple tube. Also, with the increase of nanofluid volume fraction, the maximum velocity magnitude also increased. Numerical results showed that with increasing Reynolds number, fluid temperature decreased and velocity fluctuations increased. Also, the maximum temperature in the problem was 305.74^{o}K, which occurred at Re=5 and at the wall location. The results showed that at higher Re, "pressure changes" were more intense. For example, as the Re increased from 5 to 10, the fluid pressure also increased by about 2.1 times. But by increasing the Re from 200 to 400, the fluid pressure had increased by 3.3 times. The results showed that the maximum temperature in the problem was approximately 300.95^{o}K and occurred shortly after the obstacle and near the wall. It was found that in almost all sections (except for a few exceptions), the pressure changes along the channel width were insignificant. A stagnation point was also formed in the flow, where the highest pressure in the problem occurred.

NOMENCLATURE

c	specific heat capacity
d	channel diameter
h	convection heat transfer coefficient
k	thermal conductivity
T^*	dimensionless temperature (Eq. 9)
P^*	dimensionless pressure (Eq. 10)
Re	Reynolds number
Nu	Nusselt number
$\bar{U}$	average velocity in the channel
ρ	density
μ	viscosity
φ	volume fraction of nanoparticles

Subscriptions

nf	nanofluid
p	nanoparticles
bf	base fluid

References

1. Askari, N., and Taheri, M. H. "Numerical Investigation of a MHD Natural Convection Heat Transfer Flow in a Square Enclosure with Two Heaters on the Bottom Wall", *Karafan*, **17**(1), pp. 101-121 (2020).

2. Manoram, R.B., Moorthy, R.S., and Ragunathan, R. "Investigation on influence of dimpled surfaces on heat transfer enhancement and friction factor in solar water heater", *J Therm Anal Calorim*, **145**, pp. 541–558 (2021).

3. Yadav, A. S., and Gattani, A. "Revisiting the influence of artificial roughness shapes on heat transfer enhancement", *Materials Today: Proceedings*, **62**(3), pp. 1383-1391 (2022).

4. Li, J., Chen, J., Chen, Y., et al. "Effectiveness of actively adjusting vapour-liquid in the evaporator for heat transfer enhancement", *Applied Thermal Engineering*, **200**, p. 117696 (2022).

5. Hu, Q. x., Qu, X., Peng, W., et al. "Experimental and numerical investigation of turbulent heat transfer enhancement of an intermediate heat exchanger using corrugated tubes", *International Journal of Heat and Mass Transfer*, **185**, p. 122385 (2022).

6. Xu, P., Zhou, T., Xing, J., et al. "Numerical investigation of heat-transfer enhancement in helically coiled spiral grooved tube heat exchanger", *Progress in Nuclear Energy*, **145**, p. 104132 (2022).

7. Shamsi, M.R., Akbari, O. A., Marzban, A., et al. "Increasing heat transfer of non-Newtonian nanofluid in rectangular microchannel with triangular ribs", *Physica E*, **93**, pp. 167–178 (2017).

8. Alipour, H., Karimipour, A., Safaei, M.R., et al. "Influence of T-semi attached rib on turbulent flow and heat transfer parameters of a silver-water nanofluid with different volume fractions in a three-dimensional trapezoidal microchannel", *Physica E: Low-dimensional Systems and Nanostructures*, **88**, pp. 60-76 (2017).

9. Nakhchi, M.E. "Experimental Optimization of Geometrical Parameters on Heat Transfer and Pressure Drop Inside Sinusoidal Wavy Channels", *Thermal Science and Engineering Progress*, **9**, pp. 121-131 (2018).

10. Yang, L., Du, K., and Zhang, Z. "Heat transfer and flow optimization of a novel sinusoidal minitube filled with non-Newtonian SiC/EG-water nanofluids", *International Journal of Mechanical Sciences*, **168**, p. 105310 (2020).

11. Shubham, Saikia, A., Dalal A., et al. "Thermo-hydraulic transport characteristics of non-Newtonian fluid flows through corrugated channels", *International Journal of Thermal Sciences*, **129**, pp. 201-208 (2018).

12. Outokesh, M., Moosavi, S.S., Ajarostaghi, A., et al. “Numerical evaluation of the effect of utilizing twisted tape with curved profile as a turbulator on heat transfer enhancement in a pipe”, *J Therm Anal Calorim*, **140**, pp. 1537–1553 (2020).

13. Chu, W. X., Tsai, C. A., Lee, B. H., et al. “Experimental investigation on heat transfer enhancement with twisted tape having various V-cut configurations”, *Applied Thermal Engineering*, **172**, p. 115148 (2020).

14. Ali Akbari, O., Toghraie, D., Karimipour, A., et al. “The effect of velocity and dimension of solid nanoparticles on heat transfer in non-Newtonian nanofluid”, *Physica E: Low-dimensional Systems and Nanostructures*, **86**, pp. 68-75 (2017).

15. Amrollahi, A., Rashidi, A.M., Lotfi, R., et al. “Convection heat transfer of functionalized MWNT in aqueous fluids in laminar and turbulent flow at the entrance region”, *International Communications in Heat and Mass Transfer*, **37**(6), pp. 717-723 (2010).

16. Zeinali Heris, S., Nasr Esfahany, M., and Etemad, S.Gh. “Experimental investigation of convective heat transfer of Al_2O_3/water nanofluid in circular tube”, *International Journal of Heat and Fluid Flow*, **28**(2), pp. 203-210 (2007).

17. Masoumnezhad, M., Kazemi, M.A., Askari, N., et al. “Semi-Analytical Solution of Unsteady Newtonian Fluid Flow and Heat Transfer between two Oscillation Plate under the Influence of a Magnetic Field”, *Karafan*, **18**(1), pp. 35-62 (2021)

18. Miansari, M., Aghajani, H., Zarringhalam, M., et al. “Numerical study on the effects of geometrical parameters and Reynolds number on the heat transfer behavior of carboxy-methyl cellulose/CuO non-Newtonian nanofluid inside a rectangular microchannel”, *J Therm Anal Calorim*, **144**, pp. 179–187 (2021).

19. Khetib, Y., Alahmadi, A., Alzaed, A., et al. “Application of Cylindrical Fin to Improve Heat Transfer Rate in Micro Heat Exchangers Containing Nanofluid under Magnetic Field”, *Processes*, **9**, p. 1278 (2021).

20. Abdelmalek, Z., D’Orazio, A., and Karimipour, A. “The Effect of Nanoparticle Shape and Microchannel Geometry on Fluid Flow and Heat Transfer in a Porous Microchannel”, *Symmetry*, **12**(4), p. 591 (2020).

21. Pahlevaninejad, N., Rahimi, M., and Gorzin, M. “Thermal and hydrodynamic analysis of non-Newtonian nanofluid in wavy microchannel”, *J Therm Anal Calorim*, **143**, pp. 811–825 (2021).

22. Mousa, M. H., Miljkovic, N., and Nawaz, K. “Review of heat transfer enhancement techniques for single phase flows”, *Renewable and Sustainable Energy Reviews*, **137**, p. 110566 (2021).

23. Mashoofi Maleki N., and Pourahmad S. “Heat transfer enhancement in a heated copper tube using the electromagnetic vibration method for nanofluids as working fluid: An experimental study”, *International Communications in Heat and Mass Transfer*, **141**, p. 106566 (2023).

24. Ma, L., Liu, X., Gao, Y., et al. “R410A and R32 condensation heat transfer and flow patterns inside horizontal micro-fin and 3-D enhanced tubes”, *International Communications in Heat and Mass Transfer*, **142**, p. 106638 (2023).

25. Yuan M., Liu, G., Zhang, X., et al. “Heat transfer enhancement for spiral finned tubes with triangular winglets”, *International Journal of Heat and Mass Transfer*, **205**, p. 123918 (2023).

26. Naga Ramesh, K., Sharma, T. K., and Rao, A.P. “Latest Advancements in Heat Transfer Enhancement in the Micro‑channel Heat Sinks: A Review. *Archives of Computational Methods in Engineering*, **28**, pp. 3135-3165 (2021).

27. Akbarzadeh, S., and Valipour, M.S. “Experimental study on the heat transfer enhancement in helically corrugated tubes under the non-uniform heat flux”, *J Therm Anal Calorim*, **140**, pp. 1611–1623 (2020).

28. Nguyen, Q., Bahrami, D., Kalbasi, R., et al. “Nanofluid flow through microchannel with a triangular

corrugated wall: Heat transfer enhancement against entropy generation intensification", *Mathematical Methods in the Applied Sciences*, pp. 1-14, DOI: 10.1002/mma.6705 (2020).

29. Wang, W., Li, Y., Zhang, Y., et al. "Analysis of laminar flow and heat transfer in an interrupted microchannel heat sink with different shaped ribs", *J Therm Anal Calorim*, **140**, pp. 1259–1266 (2020).

30. Zhang, K., Sun, Z., Zheng, N., et al. "Effects of the configuration of winglet vortex generators on turbulent heat transfer enhancement in circular tubes", *International Journal of Heat and Mass Transfer*, **157**, p. 119928 (2020).

31. Mehta, S.K., and Pati, S. "Analysis of thermo-hydraulic performance and entropy generation characteristics for laminar flow through triangular corrugated channel", *J Therm Anal Calorim*, **136**, pp. 49–62 (2019).

32. Zhang, L., Yan, X., Zhang, Y., et al. "Heat transfer enhancement by streamlined winglet pair vortex generators for helical channel with rectangular cross section", *Chemical Engineering and Processing - Process Intensification*, **147**, p. 107788 (2020).

33. Minea, A. A., "Uncertainties in modeling thermal conductivity of laminar forced convection heat transfer with water alumina nanofluids", *International Journal of Heat and Mass Transfer*, **68**, pp. 78–84 (2014).

34. Mukherjee, S., Jana, S., Mishra, P. C., et al. "Experimental investigation on thermo-physical properties and subcooled flow boiling performance of Al2O3/water nanofluids in a horizontal tube", *International Journal of Thermal Sciences*, **159**, p. 106581 (2021).

35. Kim, D., Kwon, Y., Cho, Y., et al. "Convective heat transfer characteristics of nanofluids under laminar and turbulent flow conditions", *Current Applied Physics*, **9**, pp. e119–e123 (2009).

Biography

Ahmad Bedram received his BSc degree in mechanical engineering (energy conversion) from Isfahan University of Technology in 2009. Also, he received his MSc and PhD degrees in mechanical engineering (energy conversion) from Sharif University of Technology in 2011 and 2015, respectively. He is an assistant professor at the Mechanical Engineering Department at Technical and Vocational University of Tehran, Iran. He has several published papers on symmetric and asymmetric droplet breakup in T-junction and similar geometries. Also, the flow pattern of micro and nano droplets is investigated in his papers. Currently, he is working on the heat transfer enhancement of nanofluids in the internal flows. The research method of his papers is computational fluid dynamic and Volume of Fluid (VOF) method for multiphase flows simulations.

Fig. 1 Geometric dimensions of the problem. The geometry is axisymmetric. The origin of the coordinates is considered in the center of the inlet section. we name this geometry: "long obstacle geometry".

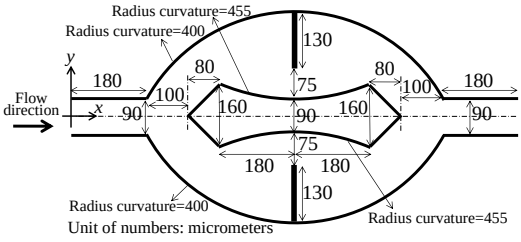

Fig. 2 Grid independency for nanofluid of water and 3.5% Al_2O_3 at Re=100 and at cross-section x=1000 µm in four grids of different sizes

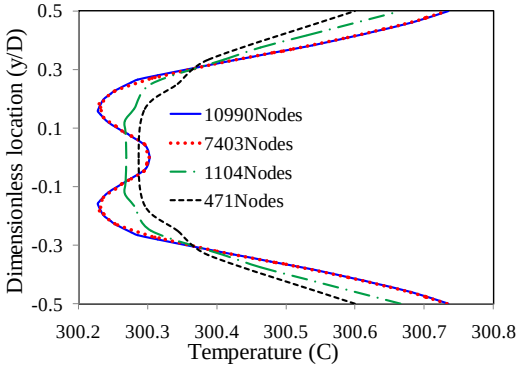

Fig. 3 Comparison of the numerical results of this paper with the experimental results of a benchmark study (Kim et al. 2009)

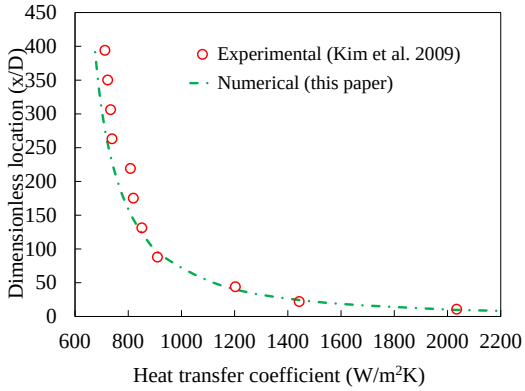

Fig. 4 Three dimensional image of the geometry. The geometry is cropped to better see the details inside the tube.

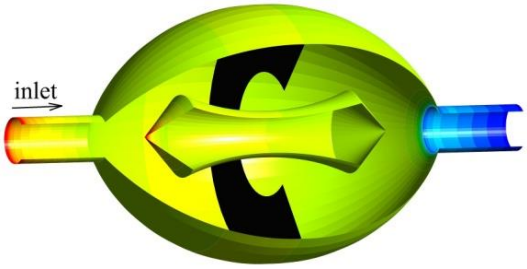

Fig. 5 Velocity magnitude profile in different nanofluid volume fractions at Reynolds number 100 and cross section x=450 µm. The origin of the coordinates and the geometric dimensions of the problem are shown in Figure 1.

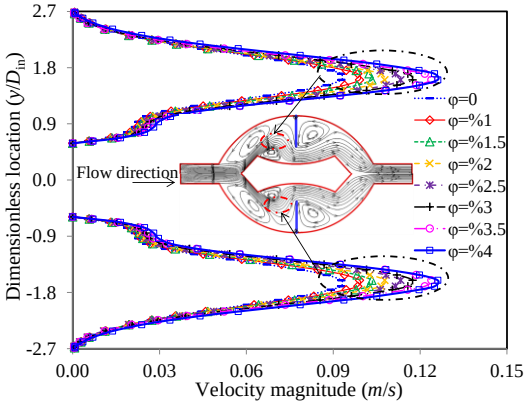

Fig. 6 Temperature profile in different nanofluid volume fractions at Reynolds number 100 and cross section x=450 µm. The origin of the coordinates and the geometric dimensions of the problem are shown in Figure 1.

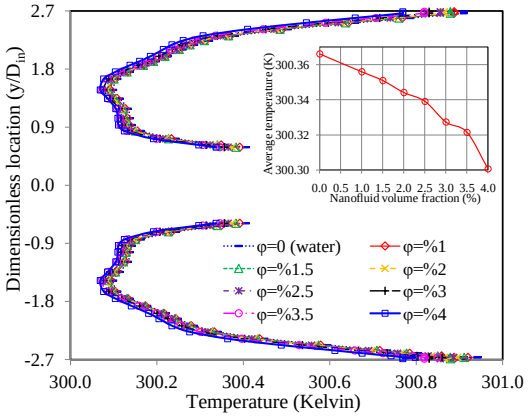

Fig. 7 Pressure profile in different nanofluid volume fractions at Reynolds number 100 and cross section x=450 µm. The origin of the coordinates and the geometric dimensions of the problem are shown in Figure 1.

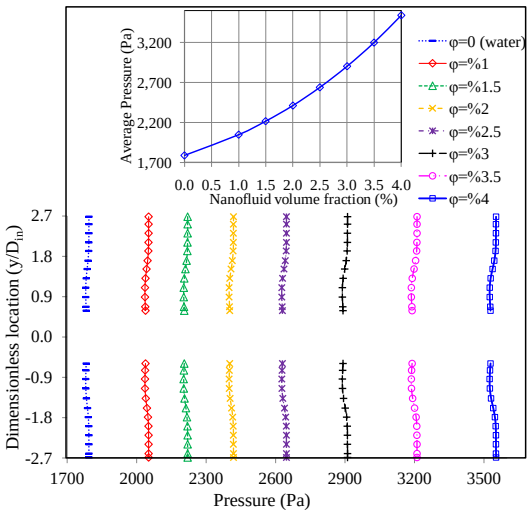

Fig. 8 "Nusselt number along the channel" in different nanofluid volume fractions. The origin of the coordinates and the geometric dimensions of the problem are shown in Figure 1.

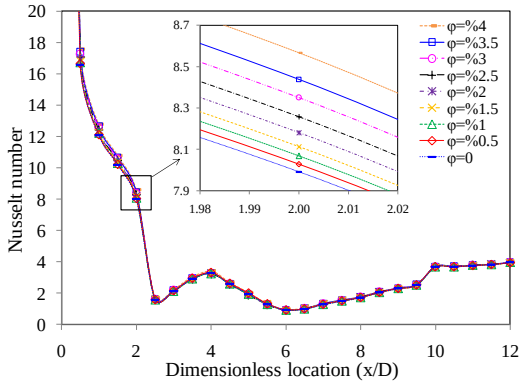

Fig. 9 Velocity magnitude profile in different Re for nanofluid with volume fraction of 3% in cross-section x=450 µm

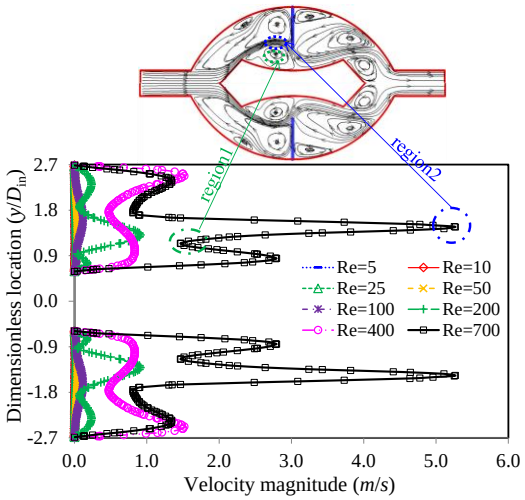

Fig. 10 Temperature profile in different Re for nanofluid with a volume fraction of 3% in cross-section x=450 µm. The velocity contour is also shown inside the diagram.

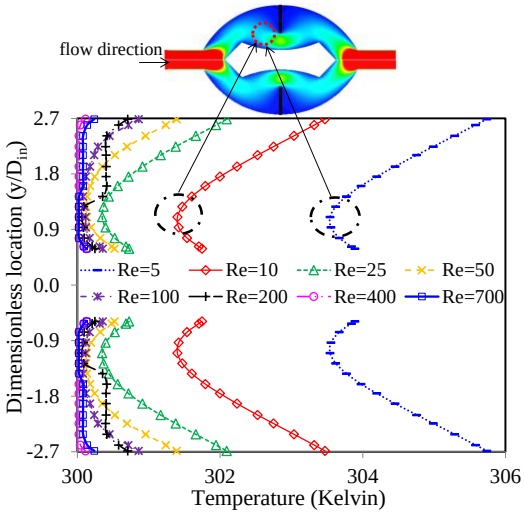

Fig. 11 Pressure profile in different Re for nanofluid with a volume fraction of 3% in cross-section x=450 µm

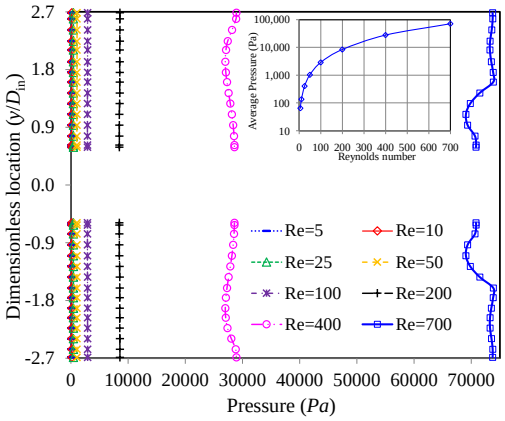

Fig. 12 “Nusselt number along the channel" in different Re. The origin of the coordinates and the geometric dimensions of the problem are shown in Figure 1. Inside the figure, the contour of the fluid velocity is drawn at a Reynolds number of 700.

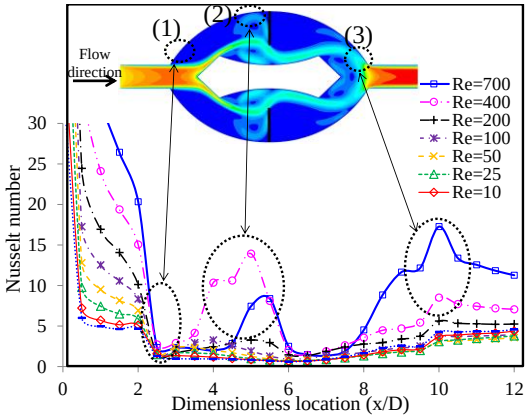

Fig. 13 Velocity magnitude contour at Reynolds number 300 and nanofluid with 3% volume fraction

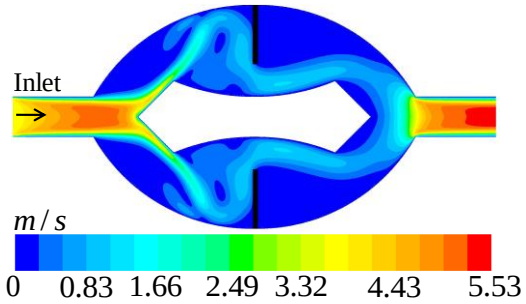

Fig. 14 Velocity magnitude profile in different sections for nanofluid with volume fraction 3% and Reynolds number 300. The selected sections and the velocity magnitude contour are shown inside the figure.

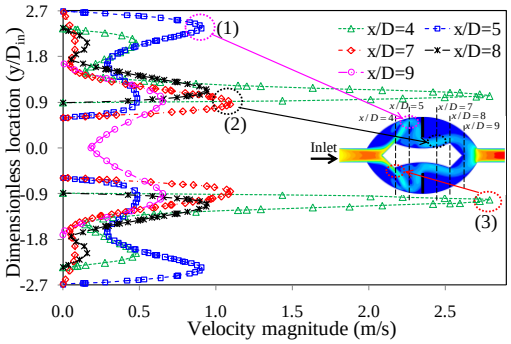

Fig. 15 Temperature contour at Reynolds number 300 and nanofluid with 3% volume fraction.

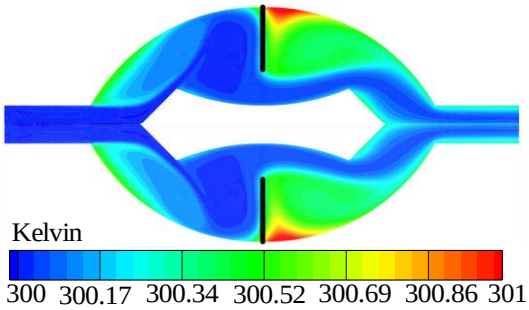

Fig. 16 Temperature profile in different sections for nanofluid with volume fraction 3% and Reynolds number 300. The selected sections and temperature contour are shown in the diagram.

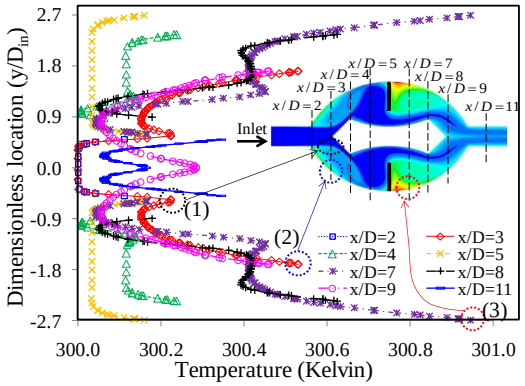

Fig. 17 Pressure contour at Reynolds number 300 and nanofluid with 3% volume fraction

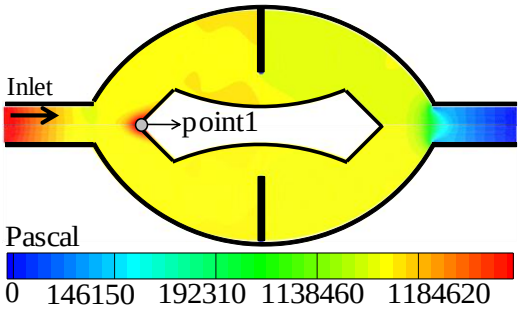

Fig. 18 Pressure profile in different sections for nanofluid with volume fraction 3% and Reynolds number 300. Selected sections and pressure contour are shown in the figure.

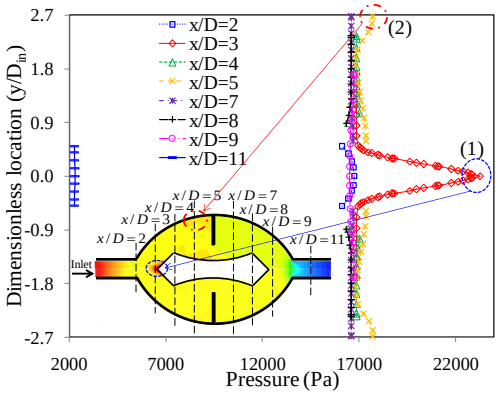

Fig. 19 Comparison of "temperature increase" and pressure drop in the proposed geometry with a simple tube at different Re. The dimensionless temperature (T^*) and dimensionless pressure (P^*) quantities are defined in equations 8 and 9, respectively.

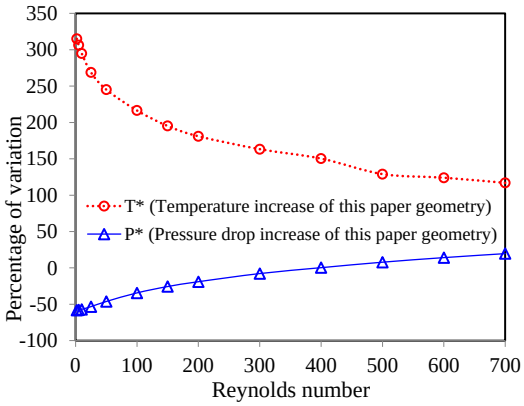

Fig. 20 Streamlines for nanofluid with 3% volume fraction at Reynolds numbers 50 to 700

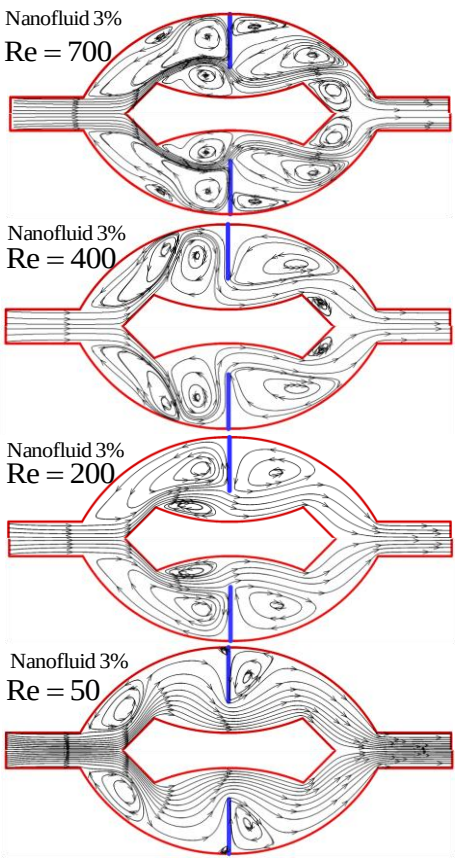

Fig. 21 Pressure drop and maximum temperature of the system for nanofluid with %3 volume fraction at $2 \leq Re \leq 700$